High-resolution cone-beam computed tomography is a fast and promising technique to quantify bone microstructure and mechanics of the distal radius

Karen Mys[1,2,*], Peter Varga[2], Filip Stockmans[3], Boyko Gueorguiev[2], Verena Neumann[2], Olivier Vanovermeire[4], Caroline E. Wyers[5,6], Joop P.W. van den Bergh[5,6,7], G. Harry van Lenthe[1]

[1] Biomechanics Section, Mechanical engineering, KU Leuven, Leuven, Belgium

[2] AO Research Institute Davos, Davos, Switzerland

[3] Muscles & Movement, Department of Development and Regeneration, KU Leuven Campus Kulak, Kortrijk, Belgium

[4] Department of Radiology, AZ Groeninge, Kortrijk, Belgium

[5] Department of Internal Medicine, VieCuri Medical Center, Venlo, the Netherlands

[6] NUTRIM School for Nutrition and Translational Research in Metabolism, Maastricht University, Maastricht, the Netherlands

[7] Rheumatology, Department of Internal Medicine, Maastricht University Medical Centre, Maastricht, the Netherlands

* Corresponding author, email address: Karen.Mys@aofoundation.org

Disclosures

Karen Mys, Peter Varga, Filip Stockmans, Boyko Gueorguiev, Verena Neumann, Olivier Vanovermeire, Caroline E. Wyers, Joop P.W. van den Bergh and G. Harry van Lenthe declare that they have no conflict of interest.

1 Short abstract

High resolution imaging of bones and joints is important for the evaluation of diseases that affect bone structure and strength. However, it remains challenging to assess the bone microstructure in clinical practice. Here we demonstrate that cone-beam CT is a promising imaging modality to enable this in clinical practice.

2 Abstract

Purpose

Obtaining high-resolution scans of bones and joints for clinical applications is challenging. HR-pQCT is considered the best technology to acquire high-resolution images of the peripheral skeleton *in vivo*, but a breakthrough for widespread clinical applications is still lacking. Recently, we showed on trapezia that CBCT is a promising alternative providing a larger FOV at a shorter scanning time. The goals of this study were to evaluate the accuracy of CBCT in quantifying trabecular bone microstructural and predicted mechanical parameters of the distal radius, the most often investigated skeletal site with HR-pQCT, and to compare it with HR-pQCT.

Methods

Nineteen radii were scanned with four scanners: (1) HR-pQCT (XtremeCT, Scanco Medical AG, @ (voxel size) $82\mu m$), (2) HR-pQCT (XtremeCT-II, Scanco, @$60.7\mu m$), (3) CBCT (NewTom 5G, Cefla, @$75\mu m$) reconstructed and segmented using in-house developed software and (4) microCT (VivaCT40, Scanco, @$19\mu m$ – gold standard). The following parameters were evaluated: predicted stiffness, strength, bone volume fraction (BV/TV) and trabecular thickness (Tb.Th), separation (Tb.Sp) and number (Tb.N).

Results

The overall accuracy of CBCT with in-house optimized algorithms in quantifying bone microstructural parameters was comparable (R^2=*0.79*) to XtremeCT (R^2=0.76) and slightly worse than XtremeCT-II (R^2=0.86) which were both processed with the standard manufacturer technique. CBCT had higher accuracy for BV/TV and Tb.Th but lower for Tb.Sp and Tb.N compared to XtremeCT. Regarding the mechanical parameters, all scanners had high accuracy ($R^2 \geq 0.96$).

Conclusion

While HR-pQCT is optimized for research, the fast scanning time and good accuracy renders CBCT a promising technique for high-resolution clinical scanning.

3 Introduction

Osteoporosis is a multi-factorial disorder of reduced bone strength and increased fragility, resulting from decrease in bone mass and deterioration of bone micro-architecture [1]. Osteoporosis induces direct medical costs over 37 billion Euro/year in Europe [2]. Quantification of bone mineral density (aBMD) using dual energy x-ray absorptiometry (DXA) combined with clinical risk factors (e.g., age, weight, gender, smoking history, alcohol use and fracture history) is the gold standard to assess the risk

of osteoporosis and subsequent fragility fractures [3], which is clinically available as the Fracture Risk Assessment (FRAX) tool [4]. However, 50% of all fractures occur in the large proportion of the population diagnosed with osteopenia, which has, following the current evaluation with FRAX, only a modest fracture risk [5, 6]. Therefore, it is important to take other bone-related factors into account, such as trabecular and cortical parameters as well as mechanical parameters, which can be assessed and quantified *in vivo* with high-resolution imaging systems.

The state-at-the-art technique to quantify bone microstructural parameters is high-resolution peripheral quantitative computed tomography (HR-pQCT) [10]. It is also the state-at-the-art to quantify bone mechanical parameters *in vivo* by making use of microFE simulations. Two imaging systems are currently available (XtremeCT and XtremeCT-II, Scanco Medical AG, Switzerland), which provide a reconstructed voxel size up to $82\ \mu m$ and $60.7 \mu m$ respectively, with a FOV (stack) of 12.6 ø x 0.9 $cm^3$and 14.0 ø x 1.0 cm^3. The rather long scan time (168 s for XtremeCT and 120 s for XtremeCT-II for one stack) increases the risk of motion artefacts and inhibits scanning of a large field of view (FOV) *in vivo*, which hampers a breakthrough in clinical practice for general applications.

A relatively new alternative imaging technique with a larger field of view is high-resolution cone-beam computed tomography (CBCT) [11]. The top range of the state-of-the-art CBCT-scanners have a high spatial resolution, large FOV, short scanning time

and low radiation dosage (e.g., a voxel size of $75\ \mu m$ and a field of view of $12x8\ cm^3$ in 18-36s). Until today, these scanners are mainly used for dental applications.

Recently, we have demonstrated on trapezia that the image quality of the CBCT device NewTom 5G (Cefla, Italy) [12] can be enhanced to reach an accuracy comparable to HR-pQCT in quantifying bone trabecular parameters [13]. This enhancement consists mainly out of an in-house developed Feldkamp-Davis-Kress (FDK) reconstruction and beam hardening correction algorithm and replaced the reconstruction program of the manufacturer completely. This was combined with an adaptive thresholding technique as segmentation tool and a direct analysis tool (Scanco Medical AG, Switzerland). The manufacturer Cefla (Italy) does not suggest a segmentation technique nor an analysis tool. Yet, not the trapezium but the distal radius is the skeletal site that is most often investigated with HR-pQCT scanners, given its confirmed relevance in osteoporosis research and for prediction of fragility fractures [14]. Therefore, the aims of this study were (1) to evaluate the accuracy of the previously developed CBCT-based analysis in quantifying bone microstructural and mechanical parameters of the distal radius and (2) to compare the accuracies of CBCT and HR-pQCT.

4 Materials and Methods

4.1 Sample collection

Nineteen radii (11 right, 8 left) of 14 female and 5 male donors aged between 25 to 93 years (mean ± SD 67.9 ± 16.2 year) were obtained from Science Care (United States). The donors donated their bodies to science. Only radii fitting in the FOV of the

VivaCT40 (Scanco Medical AG, Switzerland - diameter of 39 mm) were selected for this study. The samples were stored at -20°C and thawed prior to scanning for 3 hours.

4.2 Image acquisition and embedding

Following thawing, the radii were first soaked in room temperature water for 30 min to rewet the tissues. Afterwards the bones were double vacuum-packed and embedded in a PMMA-cylinder (46 mm diameter and 65 mm height) at 75 mm measured from the distal end that allowed reproducible positioning in the different scanners. The bone long axis was aligned with three line lasers aligned in different planes to assure centralized vertical positioning within the cylindrical embedding holder (Fig. 1a,b). The centralized alignment was essential for fitting the FOV of the microCT scanner (Fig. 1c). The distal radii were then scanned with four different scanners, by making use of custom sample holders (Fig. 1c): (1) using a HR-pQCT (XtremeCT, Scanco Medical AG, Switzerland) at a voxel size of $82\ \mu m$, (2) using a HR-pQCT (XtremeCT-II, Scanco Medical AG, Switzerland) at a voxel size of $60.7\ \mu m$, (3) using a CBCT (NewTom 5G, Cefla, Italy) scanned following the $75\ \mu m$ protocol of the scanner and reconstructed at a voxel size of $60\ \mu m$ by means of in-house developed software [12] and (4) using a small-animal microCT scanner (VivaCT40, Scanco Medical AG, Switzerland) at a voxel size of $19\ \mu m$ (Fig. 2). The microCT scanner, having the highest resolution, was used as the gold standard in all further analyses [15].

4.3 Selecting sections and volume of interest

Two adjacent sections of $9\ mm$ length were selected for each distal radius based on the microCT scans. The first section was selected strictly adjacent to the most proximal point of the subchondral endplate, aligned perpendicular to the long bone axis and termed 'subchondral section' in this study. The second section was selected directly distal to the first layer, and it mimics the measurement area recommended for clinical scanning, termed ‘standard section’ throughout this study [16].

4.4 Image segmentation

The XtremeCT, XtremeCT-II and microCT images were segmented following the standard manufacturer’s protocol which is for all of them a filtering operation followed by a global threshold. In more detail, for the XtremeCT a Laplace-Hamming filter and for the XtremeCT-II and microCT VivaCT40 a Gaussian filter were proposed by the manufacturer and used in this study with the default settings. The CBCT images were segmented using adaptive thresholding as described in Mys et al. [12]. First, a global pre-segmentation step was performed with a low global threshold and used as input for the adaptive segmentation. To reduce the noise, the pre-segmented volume was masked with a Gaussian filter (sigma of 1) followed by global thresholding with the same low threshold level. In parallel, a high global threshold was applied to select the thick bone parts (e.g., cortical bone) which would be unselected by the adaptive segmentation process. Finally, both segmentations were combined. The low and high global thresholds in the adaptive segmentation technique were optimized in steps of 5% of the highest grey value to the highest correlation for both subsections together. To avoid overoptimization, the optimization was checked on random subsets of the dataset.

158 The optimization was done separately for three parameter groups. The first group is
159 BV/TV, Tb.Sp and Tb.N, the second group is Tb.Th and the third group are the
160 mechanical parameters. The volume of interest (VOI) corresponding to trabecular bone
161 was selected automatically based on the microCT images using the masking method of
162 Buie et al. [17] as described in more detail in Mys et al. [12].
163

164 ## 4.5 Calculation of bone microstructural parameters

165 Bone volume fraction (BV/TV), trabecular thickness (Tb.Th), trabecular separation
166 (Tb.Sp) and trabecular number (Tb.N) were calculated within the VOI using the Image
167 Processing Language (IPL) software of Scanco. Following the manufacturer's
168 guidelines, the segmented XtremeCT images were analysed using the indirect bone
169 microstructural evaluation assuming a parallel plate model, whereas the segmented
170 XtremeCT-II and microCT images were analysed by means of the direct microstructural
171 analysis. For CBCT, for which no standard analysis method exists, the same direct
172 microstructural analysis was used.
173

174 ## 4.6 Calculation of bone mechanical parameters

175 Bone stiffness and strength were calculated by means of the microFE analysis software
176 ParOsol on all scans of all scanners. Prior to the analysis, component labelling was
177 applied in Matlab R2017b (The Mathworks, United States) to the segmented images so
178 that only the largest connected part (6-part connectivity) was considered. Each bone
179 voxel of the segmented images was converted to an equally sized brick element in the
180 microFE model. Consequently, the size of the brick elements was scanner-specific and

depended on the voxel size of the scan. The bone material was implemented as a homogenous linear elastic material with a Young's modulus of 15 GPa and a Poisson's ratio of 0.3. As boundary conditions, the most proximal nodes were fixed in all directions and the most distal nodes were displaced with $1\ mm$ along the longitudinal direction. The boundary conditions, together with the segmented image and the material properties, were directly written in a h5-file. This h5-file could be run directly in the voxel-based microFE-software ParOsol [18]. This technique was used for all scans of all scanners.

The microFE analyses were solved on a Hybrid Cray XC407XC50 on Piz Daint at CSCS (Switzerland) using one or two nodes each consisting of 36 CPU cores. Bone stiffness was calculated by summing the forces at the constraint proximal nodes and dividing it by the applied displacement. Bone strength was calculated using the Pistoia criterion [19]. Specifically, the bone strength was defined as the force at which 6% of the bone voxels experienced an effective strain equal or larger than 0.7%.

4.7 Image registration

In order to compare bone parameters of the different scanners, the same VOI needed to be evaluated for the microstructural bone parameters and the same boundary and loading conditions had to be applied on the microFE models. Performing the calculations on registered CT images would have resulted in loss of accuracy, because details in the microstructure would have been lost due to resampling and interpolation. To avoid this, the bone VOI mask was transformed for evaluation of the bone

204 microstructural parameters. The corresponding transformation matrices were
205 determined by spatially registering the images of the XtremeCT, XtremeCT-II and CBCT
206 to microCT using the software Amira v6.2 (Thermo Fisher Scientific, USA).
207
208 The segmented images were not rotated to generate the microFE models, but the use
209 of the custom sample holders ensured negligible misalignment. For XtremeCT, the
210 maximal axial misalignment with microCT was 2.37° (mean 1.03°, SD 0.64°), for
211 XtremeCT-II 4.07° (mean 2.19°, SD 0.83°) and for CBCT 2.78° (mean 1.98°, SD 0.52°).
212

213 ### 4.8 Statistics

214 Accuracy was quantified by comparing the results of the XtremeCT, XtremeCT-II and
215 CBCT scanners with the microCT data via linear regression analysis. Also the intercept,
216 slope and offset as well as the coefficient of determination were calculated against
217 microCT. Offset was calculated as the average difference with the microCT-based
218 value.
219 Scatter plots and Bland Altman plots were generated for a visual and quantitative
220 assessment of accuracy. All statistical tests were performed in Matlab R2017b (The
221 Mathworks, United States).
222

223 ## 5 Results

224 A summary of the bone microstructural parameters BV/TV, Tb.Th, Tb.Sp and Tb.N and
225 bone mechanical parameters, stiffness and strength is given in Table 1. Specifically, the

mean and standard deviation of all parameters are listed for microCT. Furthermore, the relative offset, slope, intercept and coefficient of determination of the *HR-pQCT and CBCT* scanners against microCT are provided. Note that the accuracy of the bone parameters reflects a combination of the scanner and the image processing afterwards on the scan.

5.1 Bone microstructural parameters

For all parameters and all scanners significant correlations ($p < 0.05$) were obtained for both bone sections. For the standard section (Fig. 3), the highest coefficient of determination for BV/TV was obtained for CBCT ($R^2 = 0.95$; Table 1). The weakest correlation for CBCT-based data was found for Tb.Th ($R^2 = 0.69$). The obtained accuracy over all bone microstructural parameters of the standard section of CBCT ($R^2 = 0.82$), was slightly better than for XtremeCT ($R^2 = 0.80$) and worse than for XtremeCT-II ($R^2 = 0.89$). The accuracy of CBCT was higher than XtremeCT for the trabecular thickness ($R^2 = 0.69$ for CBCT against $R^2 = 0.58$ for XtremeCT). For Tb.Sp, the opposite was true ($R^2 = 0.88$ for XtremeCT against $R^2 = 0.77$ for CBCT). The accuracy of CBCT versus XtremeCT-II was similar for BV/TV and for Tb.N, and slightly lower for Tb.Th and for Tb.Sp (Table 1).

For the subchondral section, lower correlations were achieved for the parameters Tb.Sp and Tb.N for all scanners (e.g., for CBCT Tb.Sp, $R^2 = 0.58$ and $R^2 = 0.77$ for the subchondral and standard section, respectively) and similar correlations for BV/TV. For Tb.Th, higher correlations were obtained for CBCT (e.g., $R^2 = 0.83$ and $R^2 = 0.69$ for

the subchondral and standard section, respectively), but this was not the case for XtremeCT and XtremeCT-II.

5.2 Bone mechanical parameters

All scanners had a high accuracy ($R^2 \geq 0.96$ for stiffness as well as for strength - Fig. 4). For stiffness of the standard section, the offset varied between 9.1% (XtremeCT-II) and 24.6% (CBCT). XtremeCT and XtremeCT-II performed slightly better ($R^2 = 0.98$ for the standard section for both scanners) than the CBCT scanner ($R^2 = 0.96$). The trends for bone strength were similar to those for bone stiffness, but the offsets were slightly higher (11.2% to 28.9%)

For the subchondral section, similar trends were observed as for the standard section, but the offsets were higher (between 1.4% and 57.3% for the stiffness and between 4.9% and 64.1% for the strength).

5.3 Optimization of segmentation parameters for CBCT

For the CBCT images, the thresholds of the adaptive segmentation had to be optimized. For the bone microstructural parameters, the optimal low global threshold for BV/TV, Tb.Sp and Tb.N varies between 22-26% of the highest grey value for those parameters optimized independently for the different sections (Fig. 5). For Tb.Th, the optimal threshold was higher and between 30-32% of the highest grey value of the image. The specific value of the high global threshold did not affect the segmentation, because the trabecular structure did not contain thick bone structures. Hence, the low global

threshold was fixed to 24% of the highest grey value for BV/TV, Tb.Sp and TB.N and to 30% for Tb.Th.

For the bone mechanical parameters of the subchondral bone section, best accuracy was obtained when a low global threshold of 24% of the highest grey value was combined with a high global threshold of 38% of the highest grey value. For the standard bone section, the optimal values were 22% and 42%, respectively. In order to standardize these settings, fixed low and high threshold values of 24% and 38% were used for the reported results of both sections.

6 Discussion

The XtremeCT-II images had higher physical resolution and the reconstructions appeared visually sharper and with more contrast than the CBCT images. Yet, the accuracies in bone microstructural and bone mechanical parameters obtained in this study with XtremeCT-II and with CBCT were very similar, except for Tb.Sp, which showed better accuracy with XtremeCT-II. We hypothesize that this can be explained as follows: the adaptive segmentation was in general able to capture the bone microstructure of the CBCT images with a high accuracy, but it was not able to detect all the small trabeculae which mainly influence the parameter Tb.Sp. The inability to detect small trabeculae is more pronounced on the CBCT scans, but also HR-pQCT has problems with it. Mainly the bones with high Tb.Sp have many of those small trabeculae, which explains why CBCT and HR-pQCT are less corresponding to each

other for these samples, mainly for the parameter Tb.Sp. The offset of the CBCT images was higher than the offset of XtremeCT-II. It is known that a lower spatial resolution will lead to higher offsets [20], which has as disadvantage that it becomes more important to calculate correction factors.

The accuracy of XtremeCT to quantify bone microstructural parameters was, in general, slightly lower compared to the other two scanners, despite that the XtremeCT images appeared visually slightly sharper than CBCT images. However, the images of the different scanners were segmented with different approaches and this may have affected the results. In particular, to achieve high accuracy with CBCT, the results of this scanner were pushed to the limits by means of software and CBCT is clearly inferior to HR-pQCT while making use of the standard reconstruction software of the CBCT scanner. We hypothesize that, by using more sophisticated segmentation approaches, the quantification accuracy could be improved for XtremeCT and potentially also for XtremeCT-II, compared to the standard method. With such optimization, the HR-pQCT scanners may achieve superior results versus CBTC. However, an actual optimisation of the segmentation technique of the XtremeCT and XtremeCT-II images was out of the scope of this study. For those devices, the manufacturers default image processing methods were used with the standard settings as these represent the tools available to the users.

To obtain good accuracy with CBCT, the reconstruction of the projection data [12] as well as the segmentation technique are critical. Yet, no standard segmentation technique exists for CBCT, so development of a segmentation technique as well as

optimization of the segmentation parameters was needed. We used an adaptive thresholding approach in which the low global threshold was optimized to obtain highest possible correlations (Fig. 5). We found that the optimal low global threshold was significantly higher for Tb.Th than for the other bone microstructural parameters. Therefore, we propose a dual adaptive segmentation technique for the microstructural parameters with one threshold when evaluating Tb.Th and another for BV/TV, Tb.Sp and Tb.N. This is a reasonable approach because for BV/TV, Tb.Sp and Tb.N it is important to quantify all trabeculae whereas for Tb.Th a more realistic thickness is important. For the microFE simulation, a low global threshold for the trabecular bone structure (24% of the highest grey value), combined with a high global threshold for the cortex (38% of the highest grey value) was optimal. Yet, the segmentation parameters of the microFE-analyses are not critical and good agreement was reached for a broad range of thresholds (data not shown). To avoid over-optimisation of the parameters, the stability of the optimisation was tested over multiple random subsamples. This test showed that the chosen parameters were reasonable and stable over those subsamples (data not shown). Yet, more analyses on larger sample sizes are required to fine-tune the segmentation technique.

De Charry et al. have already demonstrated that bone microstructural parameters of distal radii determined using the NewTom 5G (Cefla, Italy) correlated well with XtremeCT; however they have not evaluated the accuracy [21]. Their results cannot be directly compared with our findings as we evaluated the accuracy of the HR-pQCT and CBCT scanners against microCT. Still, in line with their findings, we also observed

important offsets for most parameters between the CBCT scanner versus the XtremeCT and microCT. However, it is already known that different resolutions and segmentation techniques result in different absolute values [20] and these consistent differences can be compensated for if the correction terms are known. Klintström et al. evaluated the accuracy of CBCT scanners, amongst other for the NewTom 5G (Cefla, Italy), against microCT to quantify bone microstructural [22] and mechanical parameters [23] on radius cubes and compared it to the accuracy obtained with XtremeCT, but not with the newest generation XtremeCT-II scanner. The correlations obtained in our study were higher than reported by Klinström et al. for all parameters except for Tb.Th. However, a direct comparison is difficult to make. In this study we tried to mimic the measurement area recommended for clinical scanning, while the study of Klinström et al. makes use of non-further specified cubes of trabecular bone of the distal radius with a side of 8mm. In this study we opted to make use of fresh-frozen bone samples. Klinström et al. made use of defatted bone samples and scanned them in water with a paraffin layer around the bone to mimic the soft tissue. We believe the fresh frozen situation is the more realistic one. According to our simulations (not shown) and reasoning, the paraffin mimics the positive effect of the soft tissue, namely reducing the beam hardening, without adding the degenerative *in vivo* aspects on the scan quality. In reality, the ulna will create extra artefacts and the radius is not in the centre of the scanned volume. Hence, this is the first study that evaluated the accuracy of CBCT in a clinically relevant section in the distal radius and compared it with the accuracy of XtremeCT and XtremeCT-II.

A limitation of this study was the *ex vivo* nature of the analyses. This means that imaging artefacts due to movement as well as due to the ulna and the surrounding soft tissue were not taken into account. Soft tissues would have an impact mainly on the beam hardening and scattering artefacts. However, the absence of the soft tissue in this study will have a negative effect on the beam hardening in the present analyses as in *in vivo* situations, the soft tissue acts as a filter that limits beam hardening. Motion artefacts are expected to be smaller with the shorter scanning time of CBCT versus HR-pQCT, but it has to be evaluated in future studies how these affect the images acquired with inferior resolution of CBTC compared to HR-pQCT. A second limitation is that the applied boundary conditions in the microFE-simulations do not represent realistic *in vivo* loading conditions. However, these are the standard boundary conditions used in other studies for microFE-simulations and correspond to those applied in the standard microFE analyses of the HR-pQCT software. A third limitation is that the CBCT scanner is not calibrated to bone mineral density (BMD). And a last limitation is that there is assumed in this study that the offsets are constant and hence, R^2 can be used as accuracy measurement. Larger datasets are needed to confirm this assumption.

6.1 Conclusion

We conclude that, for distal radius sections, CBCT-based microstructural and mechanical parameters calculated on our in-house processed images have comparable accuracy to HR-pQCT-based parameters assessed with the standard methods. XtremeCT-II provides slightly higher accuracy than XtremeCT and CBCT. The accuracy

of CBCT is higher for BV/TV and Tb.Th, but lower for Tb.Sp and Tb.N compared to XtremeCT

For non-clinical research, HR-pQCT seems to be the best option, because it provides the sharpest scan, while the reduced scanning time and larger FOV make CBCT an interesting technique enabling high-resolution *in vivo* scanning in clinical practice. In future, new imaging modalities combining the positive aspects of HR-pQCT, CBCT as well as the image processing techniques developed for CBCT in this research, may advance this field.

7 Acknowledgements

The authors are not compensated and there are no other institutional subsidies, corporate affiliations, or funding sources supporting this study unless clearly documented and disclosed. This research was supported by an FWO travel grant (Grant V438418N), by KU Leuven Internal Funding (Grant C24/16/027) and by the Swiss National Supercomputing Centre under project ID 891. The authors would like to thank Ursula Eberli (AO Research Institute Davos, Davos, Switzerland) for assistance with the IPL software and Dieter Wahl (AO Research Institute Davos, Davos, Switzerland) for assistance with the development of scanning techniques and the development of scanner specific holders.

Authors' contributions

Study design: KM, PV, FS, BG and HVL. Data collection: KM, VN, OV, CW and JVB. Data analysis: KM and PV. Data interpretation: KM, PV, FS, BG and HVL. Drafting

manuscript: KM. Revising manuscript content: PV, FS, BG, VN, OV, CW, JVB and HVL. Approving final version of manuscript: KM, PV, FS, BG, VN, OV, CW, JPV and HVL. KM takes responsibility for the integrity of the data analysis.

8 References

1. Peacock M, Turner CH, Econs MJ, Foroud T (2002) Genetics of Osteoporosis. Endocr Rev 23:303–326. https://doi.org/10.1007/s10354-005-0249-2
2. Hernlund E, Svedbom A, Ivergård M, et al (2013) Osteoporosis in the European Union: Medical management, epidemiology and economic burden: A report prepared in collaboration with the International Osteoporosis Foundation (IOF) and the European Federation of Pharmaceutical Industry Associations (EFPIA). Arch Osteoporos 8:. https://doi.org/10.1007/s11657-013-0136-1
3. Blake GM, Fogelman I (2007) The role of DXA bone density scans in the diagnosis and treatment of osteoporosis. Postgrad Med J 83:509–517. https://doi.org/10.1136/pgmj.2007.057505
4. Kanis JA, Johnell O, Oden A, et al (2008) FRAX^{TM} and the assessment of fracture probability in men and women from the UK. Osteoporos Int 19:385–397. https://doi.org/10.1007/s00198-007-0543-5
5. Sanders KM, Nicholson GC, Watts JJ, et al (2006) Half the burden of fragility fractures in the community occur in women without osteoporosis. When is fracture prevention cost-effective? Bone 38:694–700. https://doi.org/10.1016/j.bone.2005.06.004
6. Schuit SCE, Van Der Klift M, Weel AEAM, et al (2004) Fracture incidence and association with bone mineral density in elderly men and women: The Rotterdam Study. Bone 34:195–202. https://doi.org/10.1016/j.bone.2003.10.001
7. Verhulp E, Rietbergen B Van, Müller R, Huiskes R (2008) Indirect determination of trabecular bone effective tissue failure properties using micro-finite element simulations. 41:1479–1485. https://doi.org/10.1016/j.jbiomech.2008.02.032

8. Macneil JA, Boyd SK (2008) Bone strength at the distal radius can be estimated from high-resolution peripheral quantitative computed tomography and the finite element method. Bone 42:1203–1213. https://doi.org/10.1016/j.bone.2008.01.017
9. Graeff C, Marin F, Petto H, et al (2013) High resolution quantitative computed tomography-based assessment of trabecular microstructure and strength estimates by finite-element analysis of the spine, but not DXA, reflects vertebral fracture status in men with glucocorticoid-induced osteoporosis. Bone 52:568–577. https://doi.org/10.1016/j.bone.2012.10.036
10. Müller R, Hildebrand T, Rüegsegger P (1994) Non-invasive bone biopsy: A new method to analyse and display the three-dimensional structure of trabecular bone. Phys Med Biol 39:145–164. https://doi.org/10.1088/0031-9155/39/1/009
11. De Cock J, Mermuys K, Goubau J, et al (2012) Cone-beam computed tomography: A new low dose, high resolution imaging technique of the wrist, presentation of three cases with technique. Skeletal Radiol 41:93–96. https://doi.org/10.1007/s00256-011-1198-z
12. Mys K, Stockmans F, Vereecke E, van Lenthe GH (2018) Quantification of bone microstructure in the wrist using cone-beam computed tomography. Bone 114:206–214. https://doi.org/10.1016/j.bone.2018.06.006
13. Mys K, Varga P, Gueorguiev B, et al (2018) A comparative analysis between cone- beam computed tomography and high- resolution peripheral computed tomography for the quantification of bone microstructure in the wrist
14. Elizabeth J S, Biver E, Burt L, et al (2019) Cortical and trabecular bone microarchitecture predicts incident fracture independently of DXA bone minderal

density and FRAX in older women and men: The Bone Microarchitecture International Consortium (BoMIC). 7:34–43. https://doi.org/10.1016/S2213-8587(18)30308-5.Cortical

15. Mys K, Varga P, Gueorguiev B, et al (2019) Correlation Between Cone-Beam Computed Tomography and High-Resolution Peripheral Computed Tomography for Assessment of Wrist Bone Microstructure. J Bone Miner Res 34:867–874. https://doi.org/10.1002/jbmr.3673

16. MacNeil JA, Boyd SK (2007) Accuracy of high-resolution peripheral quantitative computed tomography for measurement of bone quality. Med Eng \& Phys 29:1096–1105. https://doi.org/10.1016/j.medengphy.2006.11.002

17. Buie HR, Campbell GM, Klinck RJ, et al (2007) Automatic segmentation of cortical and trabecular compartments based on a dual threshold technique for in vivo micro-CT bone analysis. Bone 41:505–515. https://doi.org/10.1016/j.bone.2007.07.007

18. Flaig C (2012) A highly scalable memory efficient multigrid solver for micro-finite element analyses. ETH Zurich

19. Pistoia W, van Rietbergen B, Lochmüller E-M, et al (2002) Estimation of distal radius failure load with micro-finite element analysis models based on three-dimensional peripheral quantitative computed tomography images. Bone 30:842–848

20. Kothari M, Keaveny TM, Lin JC, et al (1998) Impact of spatial resolution on the prediction of trabecular architecture parameters. Bone 22:437–443. https://doi.org/10.1016/S8756-3282(98)00031-3

21. de Charry C, Boutroy S, Ellouz R, et al (2016) Clinical cone beam computed tomography compared to high-resolution peripheral computed tomography in the assessment of distal radius bone. Osteoporos Int 27:3073–3082. https://doi.org/10.1007/s00198-016-3609-4

22. Klintström E, Klintström B, Moreno R, et al (2016) Predicting trabecular bone stiffness from clinical cone-beam CT and HR-pQCT Data; an in vitro study using finite element analysis. PLoS One 11:1–19. https://doi.org/10.1371/journal.pone.0161101

23. Klintström E, Klintström B, Pahr D, et al (2018) Direct Estimation of Trabecular Bone Stiffness Using Cone-Beam Computed Tomography. Oral Surg Oral Med Oral Pathol Oral Radiol 126:72–82. https://doi.org/10.1016/j.oooo.2018.03.014

9 Figures

Figure 1: Demonstration of the sample preparation steps and scanning. The radii were (a) aligned in the center of a FOV of 3.9 cm by making use of 3 lasers, (b) were embedded in a PMMA ring starting 7.5 cm from the distal end of the bone and (c) scanned by making use of scanner-specific holders to allow scanning of all the radii in the same orientation in all scanners. The VivaCT40-holder is shown on the picture.

Figure 2: The reconstructed images on the left and the corresponding segmented images on the right. (a) MicroCT VivaCT40 (Scanco Medical AG, Switzerland); (b)

505 XtremeCT (Scanco Medical AG, Switzerland) image segmented using the standard
506 Scanco technique (Laplace-Hamming filter + fixed threshold); (c) XtremeCT-II (Scanco
507 Medical AG, Switzerland) image segmented using the standard Scanco technique
508 (Gaussian filter + fixed threshold); (d) in-house reconstructed CBCT NewTom 5G
509 (Cefla, Italy) image with beam-hardening correction and segmented using adaptive
510 segmentation.
511
512
513 **Figure 3**: Scatter plots and Bland-Altman plots between MicroCT and XtremeCT,
514 XtremeCT-II and CBCT for the standard section for bone volume fraction (BV/TV),
515 trabecular thickness (Tb.Th), trabecular separation (Tb.Sp) and trabecular number
516 (Tb.N). The solid line on the scatter plot indicates the line y = x.
517
518 **Figure 4**: Scatter plots and Bland-Altman plots between MicroCT and XtremeCT,
519 XtremeCT-II and CBCT for the standard section for bone stiffness and strength. The
520 solid line on the scatter plot indicates the line y = x.
521
522 **Figure 5**: Coefficient of determination (R^2) as a function of threshold in the adaptive
523 segmentation to quantify the bone microstructural parameters with CBCT of the
524 subchrondal section as well as the standard section. Threshold is expressed as a
525 percentage of the maximum grey level. For the bone microstructural parameters BV/TV,
526 Tb.Sp and Tb.N a low global threshold between 22-26% of the highest grey value
527 provides optimal correlation. For the Tb.Th a higher threshold between 30-32% of the

highest grey value provides optimal correlation. The selected threshold (24% for BV/TV, Tb.Sp and Tb.N and 30% for Tb.Th) is indicated on every graph with a thicker marker. Note that this does not correspond for every parameter with the highest correlation.

10 Tables

Table 1: Mean and standard deviation for the microstructural parameters BV/TV, Tb.Th, Tb.Sp and Tb.N and bone mechanical parameters stiffness and strength as determined by microCT for the subchondral section as well as for the standard section. For XtremeCT, XtremeCT-II and CBCT, the slope, intercept, relative offset (in percentage against microCT) and the coefficient of determination (R^2) are given with respect to microCT. For XtremeCT and XtremeCT-II, the standard segmentation techniques were used and for CBCT an adaptive segmentation technique was used.
*For XtremeCT, the offset is not reported because due to the indirect analysis, the offset is made artificially low and not comparable with the other scanners which are analysed with a direct analysis method.

(a) *Aligning*

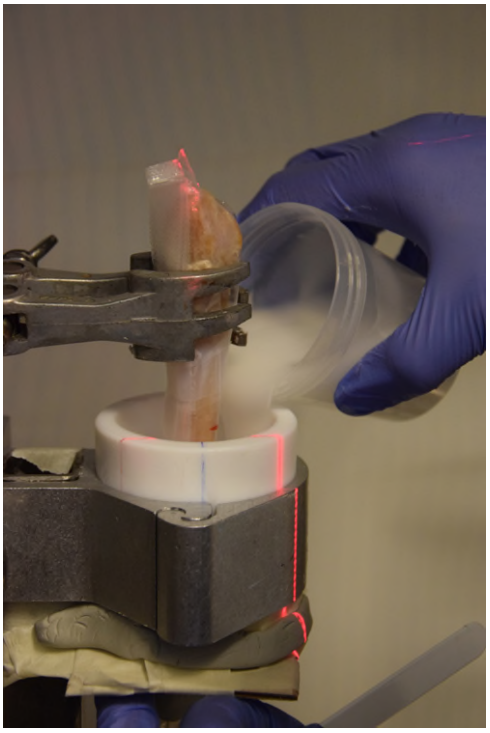

(b) *Imbedding*

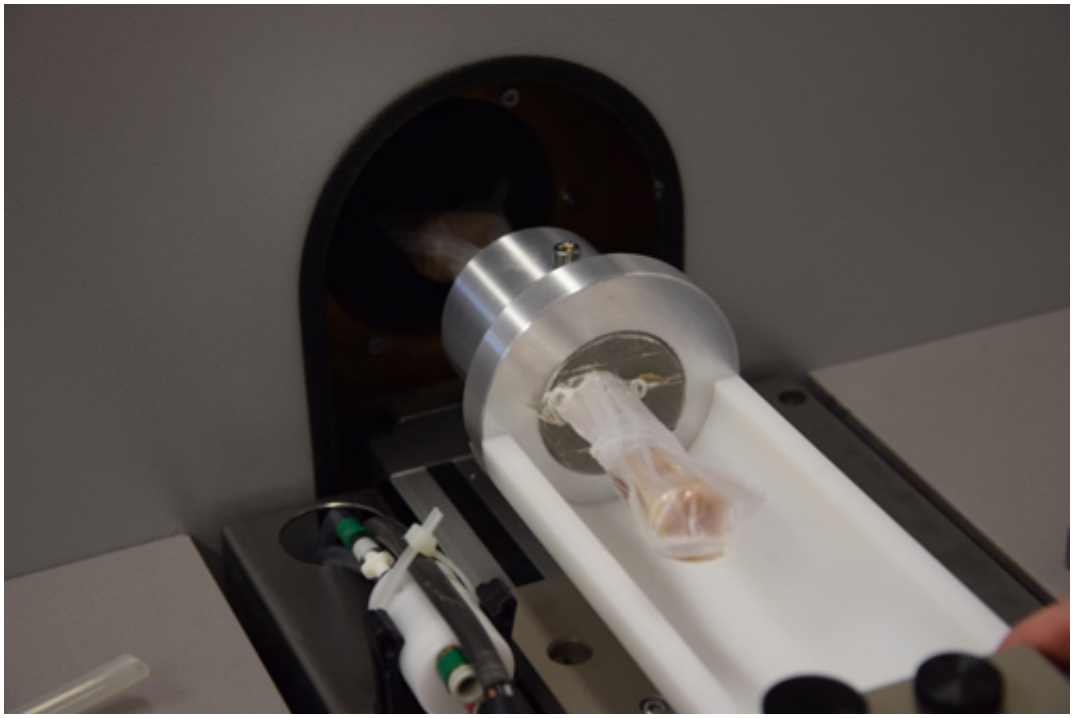

(c) *Scanning*

Figure 1: *Demonstration of the sample preparation steps and scanning. The radii were (a) aligned in the center of a FOV of 3.9 cm by making use of 3 lasers, (b) were embedded in a PMMA ring starting 7.5 cm from the distal end of the bone and (c) scanned by making use of scanner-specific holders to allow scanning of all the radii in the same orientation in all scanners. The VivaCT40-holder is shown on the picture.*

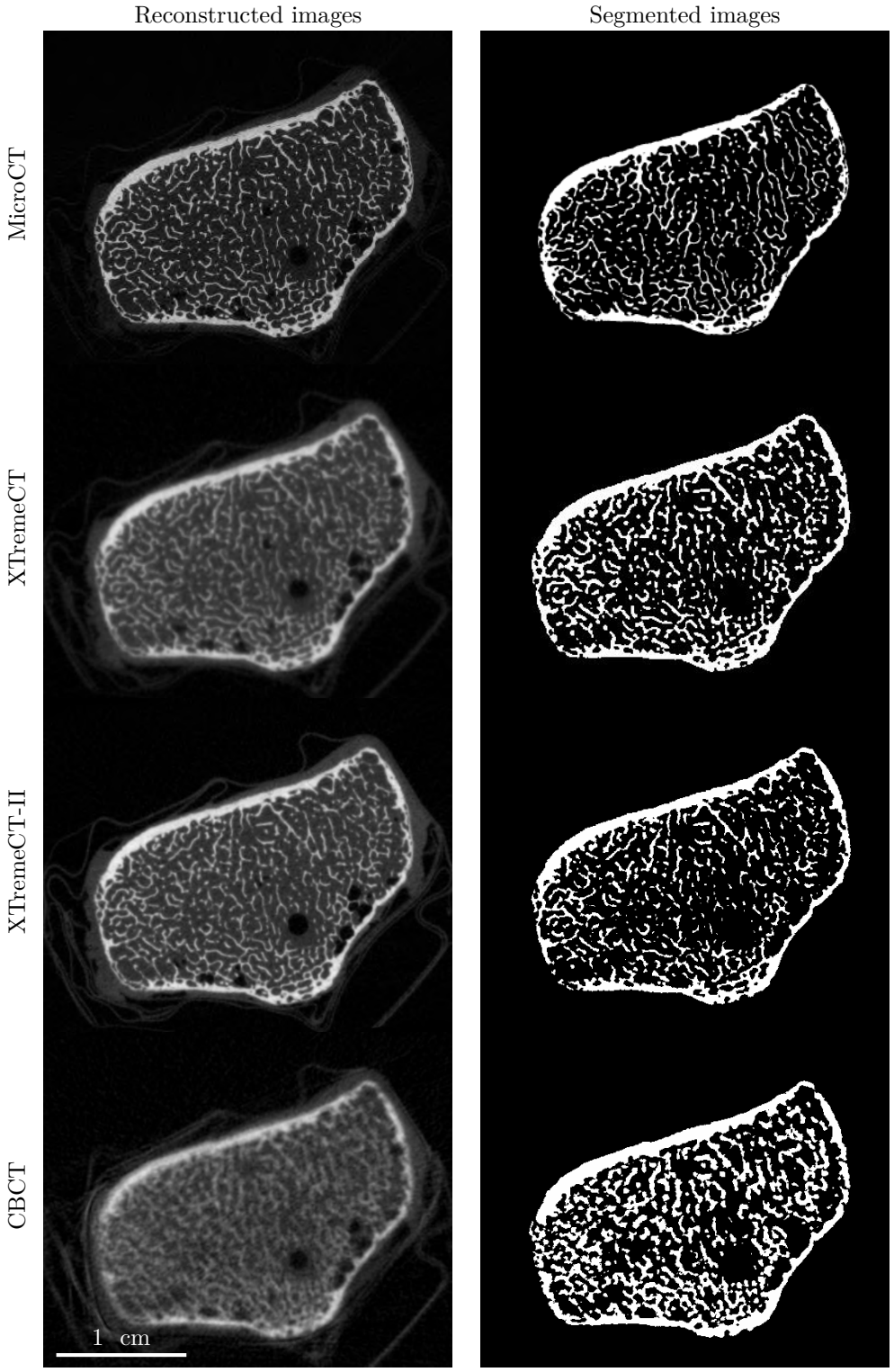

Figure 2: *The reconstructed images on the left and the corresponding segmented images on the right. (a) MicroCT VivaCT40 (Scanco Medical AG, Switzerland); (b) XTremeCT (Scanco Medical AG, Switzerland) image segmented using the standard Scanco technique (Laplace-Hamming filter + fixed threshold); (c) XTremeCT-II (Scanco Medical AG, Switzerland) image segmented using the standard Scanco technique (Gaussian filter + fixed threshold); (d) in-house reconstructed CBCT NewTom 5G (Cefla, Italy) image with beam-hardening correction and segmented using adaptive segmentation.*

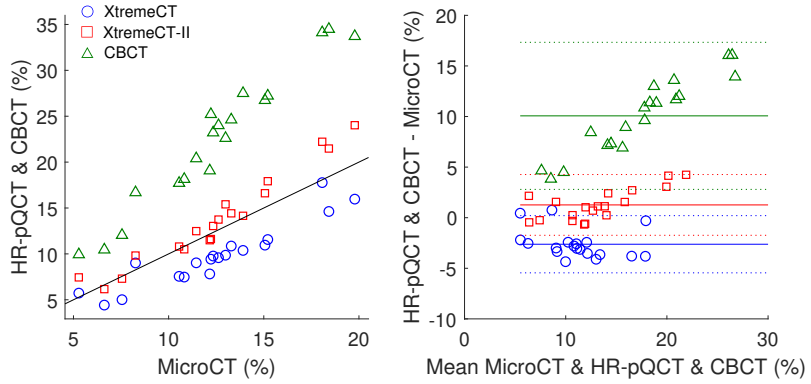

(a) *Bone volume fraction (BV/TV)*

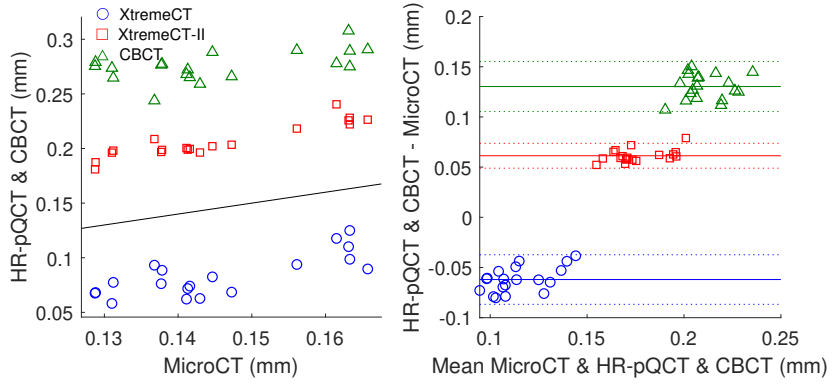

(b) *Trabecular thickness (Tb.Th)*

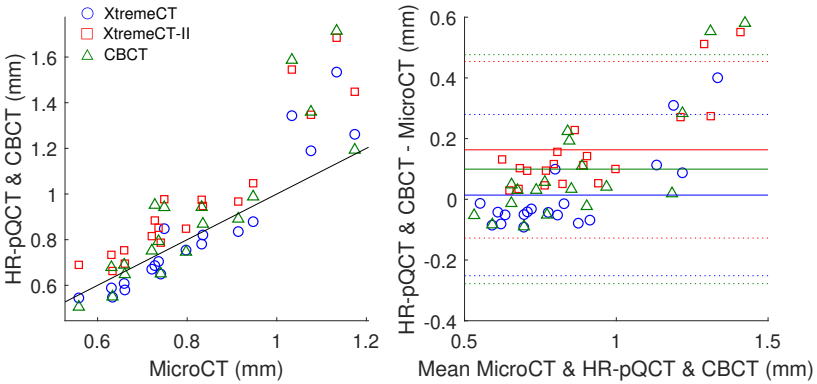

(c) *Trabecular separation (Tb.Sp)*

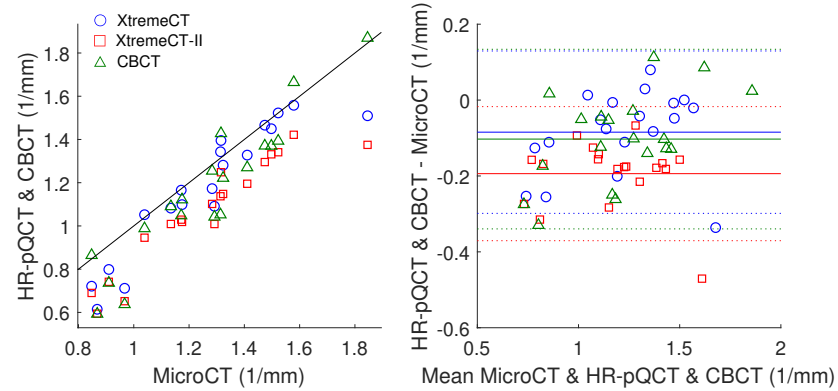

(d) *Trabecular number (Tb.N)*

Figure 3: *Scatter plots and Bland-Altman plots between MicroCT and XTremeCT, XTremeCT-II and CBCT for the standard section for bone volume fraction (BV/TV), trabecular thickness (Tb.Th), trabecular separation (Tb.Sp) and trabecular number (Tb.N). The solid line on the scatter plot indicates the line $y = x$.*

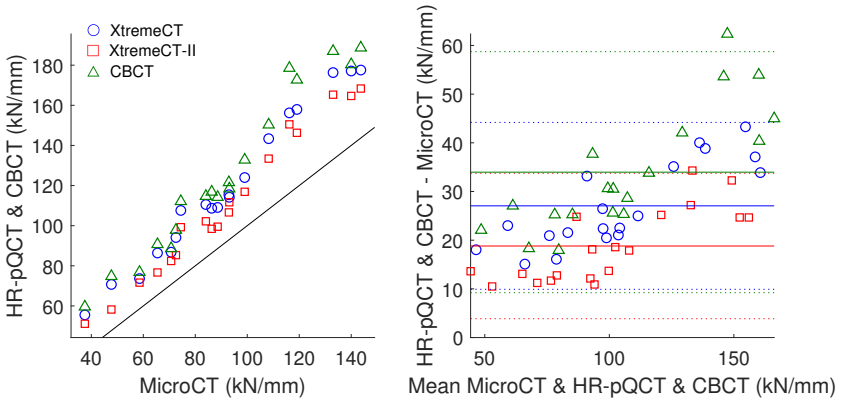

(a) *Stiffness*

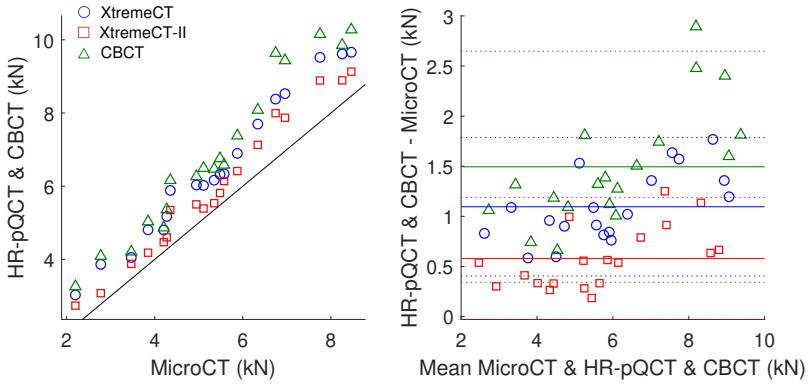

(b) *Strength*

Figure 4: *Scatter plots and Bland-Altman plots between MicroCT and XTremeCT, XTremeCT-II and CBCT for the standard section for bone stiffness and strength. The solid line on the scatter plot indicates the line $y = x$.*

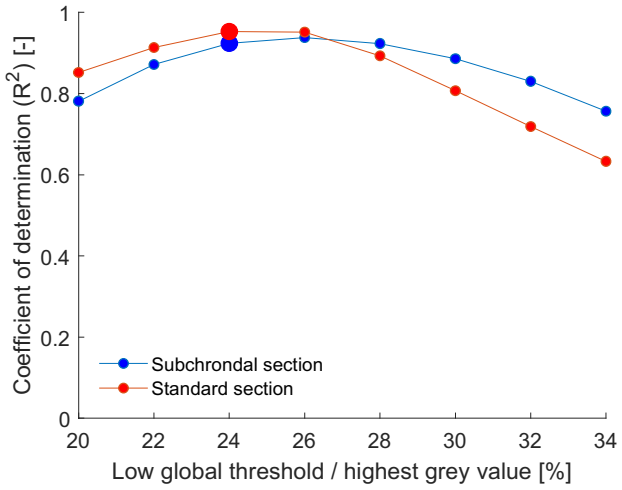

(a) *Bone volume fraction (BV/TV)*

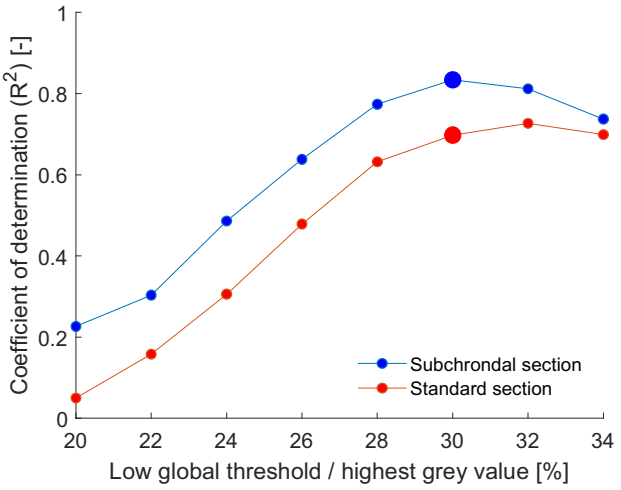

(b) *Trabecular thickness (Tb.Th)*

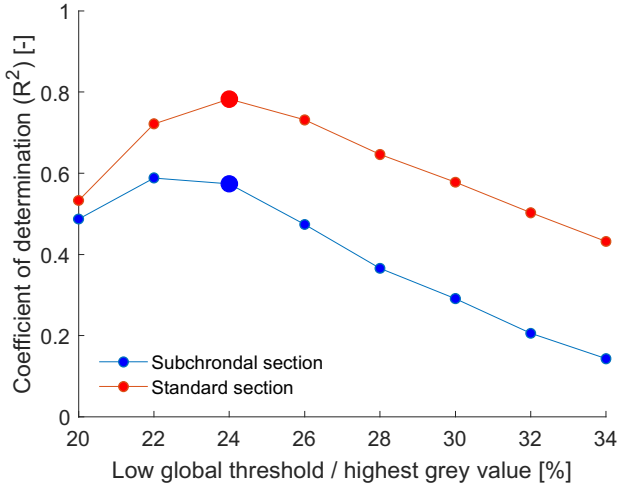

(c) *Trabecular separation (Tb.Sp)*

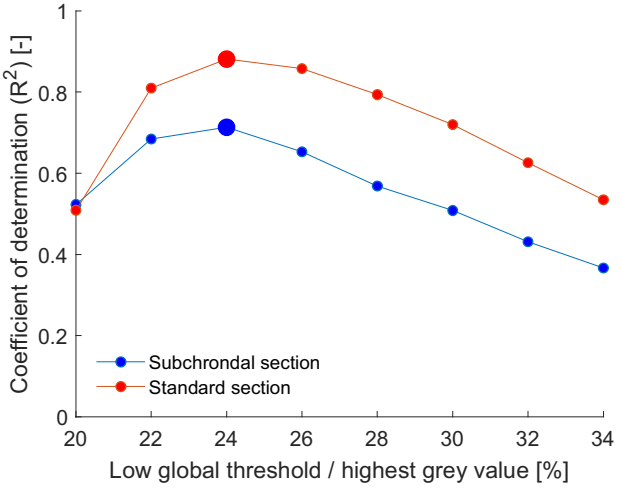

(d) *Trabecular number (Tb.N)*

Figure 5: *Coefficient of determination (R^2) as a function of threshold in the adaptive segmentation to quantify the bone microstructural parameters with CBCT of the subchrondal section as well as the standard section. Threshold is expressed as a percentage of the maximum grey level. For the bone microstructural parameters BV/TV, Tb.Sp and Tb.N a low global threshold between $22-26\%$ of the highest grey value provides optimal correlation. For the Tb.Th a higher threshold between $30-32\%$ of the highest grey value provides optimal correlation. The selected threshold (24% for BV/TV, Tb.Sp and Tb.N and 30% for Tb.Th) is indicated on every graph with a thicker marker. Note that this does not correspond for every parameter with the highest correlation.*

		MicroCT		XtremeCT				XtremeCT-II				CBCT			
		Mean	SD	Intercept	Slope	Offset	R^2	Intercept	Slope	Offset	R^2	Intercept	Slope	Offset	R^2
Subchondral	BV/TV [%]	16.03	3.36	-0.45	0.83	/*	0.88	-1.84	1.25	7.85	0.96	-0.62	1.86	84.44	0.92
	Tb.Th [mm]	0.15	0.01	-0.08	1.14	/*	0.45	0.04	1.12	25.69	0.84	0.19	0.60	53.57	0.83
	Tb.Sp [mm]	0.70	0.11	-0.40	1.50	/*	0.82	-0.31	1.58	9.02	0.75	-0.42	1.63	-5.07	0.58
	Tb.N [1/mm]	1.45	0.22	-0.13	1.03	/*	0.75	-0.06	0.90	-14.45	0.75	-0.31	1.16	-0.50	0.71
	Average			-0.26	1.13	/*	0.73	-0.54	1.21	7.03	0.83	-0.29	1.31	33.11	0.76
	Stiffness [kN/mm]	77.97	27.63	6.00	1.23	35.13	0.99	1.41	1.19	1.39	0.98	4.53	1.32	57.31	0.97
	Strength [kN]	4.23	1.40	0.45	1.12	40.86	0.98	0.08	1.09	4.93	0.99	0.34	1.21	64.08	0.97
	Average			3.23	1.18	38.00	0.99	0.74	1.14	3.16	0.99	2.44	1.27	60.70	0.97
Standard	BV/TV [%]	12.45	3.89	-1.65	0.83	/*	0.86	-5.84	1.46	9.47	0.94	-0.48	1.88	80.13	0.95
	Tb.Th [mm]	0.15	0.01	-0.05	0.94	/*	0.58	0.04	1.17	23.91	0.85	0.18	0.67	48.89	0.69
	Tb.Sp [mm]	0.82	0.18	-0.16	1.17	/*	0.88	-0.07	1.26	13.32	0.88	-0.20	1.31	5.25	0.77
	Tb.N [1/mm]	1.26	0.27	0.04	0.93	/*	0.86	0.07	0.81	-15.81	0.88	-0.28	1.19	-9.19	0.88
	Average			-0.45	0.97	/*	0.80	-1.45	1.17	7.72	0.89	-0.20	1.26	31.27	0.82
	Stiffness [kN/mm]	101.13	33.37	-1.88	1.53	17.88	0.98	-24.11	1.52	9.10	0.98	0.41	1.73	24.59	0.96
	Strength [kN]	5.37	1.76	0.04	1.40	21.70	0.98	-1.20	1.37	11.20	0.98	0.09	1.61	28.94	0.96
	Average			-0.92	1.46	19.79	0.98	-12.65	1.44	10.15	0.98	0.25	1.67	26.77	0.96